

^{68}Ga - and ^{177}Lu -Labeled PSMA I&T: Optimization of a PSMA-Targeted Theranostic Concept and First Proof-of-Concept Human Studies

Martina Weineisen¹, Margret Schottelius¹, Jakub Simecek^{1,2}, Richard P. Baum³, Akin Yildiz⁴, Seval Beykan⁵, Harshad R. Kulkarni³, Michael Lassmann⁵, Ingo Klette³, Matthias Eiber⁶, Markus Schwaiger⁶, and Hans-Jürgen Wester¹

¹Pharmaceutical Radiochemistry, Technische Universität München, Garching, Germany; ²Scintomics GmbH, Fürstenfeldbruck, Germany; ³Theranostics Center for Molecular Radiotherapy and Molecular Imaging (PET/CT), Zentralklinik Bad Berka, Bad Berka, Germany; ⁴Department of Nuclear Medicine, Medstar Hospital Cancer Center, Antalya, Turkey; ⁵Department of Nuclear Medicine, University of Würzburg, Würzburg, Germany; and ⁶Department of Nuclear Medicine, Klinikum Rechts der Isar, Technische Universität München, Munich, Germany

On the basis of the high and consistent expression of prostate-specific membrane antigen (PSMA) in metastatic prostate cancer (PC), the goal of this study was the development, preclinical evaluation, and first proof-of-concept investigation of a PSMA inhibitor for imaging and therapy (PSMA I&T) for ^{68}Ga -based PET and ^{177}Lu -based endoradiotherapeutic treatment in patients with metastatic and castration-resistant disease. **Methods:** PSMA I&T was synthesized in a combined solid phase and solution chemistry strategy. The PSMA affinity of ^{68}Ga -/ ^{177}Lu -PSMA I&T was determined in a competitive binding assay using LNCaP cells. Internalization kinetics of ^{68}Ga - and ^{177}Lu -PSMA I&T were investigated using the same cell line, and biodistribution studies were performed in LNCaP tumor-bearing CD-1 *nu/nu* mice. Initial human PET imaging studies using ^{68}Ga -PSMA I&T, as well as endoradiotherapeutic treatment of 2 patients with metastatic PC using ^{177}Lu -PSMA I&T, were performed. **Results:** PSMA I&T and its cold gallium and lutetium analog revealed nanomolar affinity toward PSMA. The DOTAGA (1,4,7,10-tetraazacyclododecane-1-(glutamic acid)-4,7,10-triacetic acid) conjugate PSMA I&T allowed fast and high-yield labeling with $^{68}\text{Ga}^{\text{III}}$ and $^{177}\text{Lu}^{\text{III}}$. Uptake of ^{68}Ga -/ ^{177}Lu -PSMA I&T in LNCaP tumor cells is highly efficient and PSMA-specific, as demonstrated by competition studies both in vitro and in vivo. Tumor targeting and tracer kinetics in vivo were fast, with the highest uptake in tumor xenografts and kidneys (both PSMA-specific). First-in-human ^{68}Ga -PSMA I&T PET imaging allowed high-contrast detection of bone lesions, lymph node, and liver metastases. Endoradiotherapy with ^{177}Lu -PSMA I&T in 2 patients was found to be effective and safe with no detectable side effects. **Conclusion:** ^{68}Ga -PSMA I&T shows potential for high-contrast PET imaging of metastatic PC, whereas its ^{177}Lu -labeled counterpart exhibits suitable targeting and retention characteristics for successful endoradiotherapeutic treatment. Prospective studies on larger cohorts of patients are warranted and planned.

Key Words: prostate-specific membrane antigen; PSMA I&T; ^{68}Ga ; ^{177}Lu ; prostate cancer

J Nucl Med 2015; 56:1169–1176
DOI: 10.2967/jnumed.115.158550

Besides radiopharmaceuticals that address metabolic processes, approaches focusing on disease-specific targets (1,2) are increasingly important for cancer diagnosis and treatment with radiopharmaceuticals. On prostate cancer (PC) cells, the cell surface enzyme prostate-specific membrane antigen (PSMA), also known as glutamate carboxypeptidase II or *N*-acetyl-L-aspartyl-L-glutamate peptidase, is highly upregulated, whereas it shows low or no expression in the normal prostate (3). PSMA expression correlates with the malignancy of the disease, being further increased in metastatic and hormone-refractory patients (4). As a consequence, PSMA has attracted attention as a target for molecular imaging and for targeted radioligand therapy, especially in metastatic castrate-resistant prostate cancer (mCRPC).

For imaging of PC, a variety of selective small-molecule PSMA inhibitors, labeled with a broad range of radionuclides for PET and SPECT, have been evaluated preclinically in recent years (5–13). Among these, ^{18}F -DCFBC (*N*-[*N*-[(*S*)-1,3-dicarboxypropyl] carbamoyl]-4- ^{18}F -fluorobenzyl-L-cysteine) (7), ^{123}I -MIP-1072 ((*S*)-2-(3-((*S*)-1-carboxy-5-(4-iodobenzylamino)pentyl)ureido)pentanedioic acid) and ^{123}I -MIP-1095 ((*S*)-2-(3-((*S*)-1-carboxy-5-(3-(4-iodophenyl)ureido)pentyl)ureido)pentanedioic acid) (9), Glu-NH-CO-NH-Lys(Ahx)- ^{68}Ga -HBED-CC (^{68}Ga -PSMA-HBED-CC) (11), and $^{99\text{m}}\text{Tc}$ -MIP-1404 ((7*S*,12*S*,16*S*)-1-(1-(2-(bis(carboxymethyl)amino)-2-oxoethyl)-1*H*-imidazol-2-yl)-2-((1-(2-(bis(carboxymethyl)amino)-2-oxoethyl)-1*H*-imidazol-2-yl)methyl)-9,14-dioxo-2,8,13,15-tetrazaoctadecane-7,12,16,18-tetracarboxylic acid) (12) have already been successfully applied in first patient PET or SPECT studies (14–17). Despite certain differences between these ligands in overall pharmacokinetics, all these compounds allow sensitive detection of PC lesions, thus improving imaging and therapy planning.

As long as the disease is restricted to the prostate, surgery and radiation therapy exhibit high efficacy (18) in therapy of PC. Treatment options for PC patients with metastatic disease are androgen-deprivation therapy and chemotherapy (19). However, these

Received Mar. 31, 2015; revision accepted Jun. 2, 2015.

For correspondence or reprints contact: Martina Weineisen, Pharmaceutical Radiochemistry, Technische Universität München, Walther-Meißner-Strasse 3, 85748 Garching, Germany.

E-mail: martina.weineisen@tum.de

Published online Jun. 18, 2015.

COPYRIGHT © 2015 by the Society of Nuclear Medicine and Molecular Imaging, Inc.

therapies cause potentially serious adverse effects. The calcium mimetic α -emitter ^{223}Ra -radium dichloride (Xofigo; Bayer AG) was recently approved. Xofigo is indicated in patients with mCRPC that has spread to bones (improved overall survival by 3.6 mo) (20). Thus, there is a major need for additional therapeutic options for patients with soft-tissue metastasizing disease.

^{111}In -capromab pendetide (ProstaScint; Cytogen Corp.) is a Food and Drug Administration–approved murine monoclonal antibody for radioimmunoscintigraphy in PC patients (21), which is directed against the intracellular domain of PSMA. To increase uptake and sensitivity (22), antibodies against the extracellular domain, for example, J591, its humanized analog huJ591, and a minibody version of huJ591, have been developed. For radioimmunotherapy, J591 was labeled with β emitters (^{90}Y , ^{177}Lu) and evaluated in patients with mCRPC (23). Patient survival could be prolonged for 9.9 mo using ^{177}Lu -J591 (24).

In a first step toward the development of small-molecule PSMA-targeting theranostics with fast pharmacokinetics and high PSMA affinity, we recently introduced (3*S*,7*S*)-29,32-dibenzyl-5,13,20,28,31,34-hexaoxo-37-(4,7,10-tris(carboxymethyl)-1,4,7,10-tetraazacyclododecan-1-yl)-4,6,12,21,27,30,33-heptaazahaptatriacontane-1,3,7,26,37-pentacarboxylic acid (DOTAGA-FFK (Sub-KuE) (13); Fig. 1; DOTAGA is 1,4,7,10-tetraazacyclododecane-1-(glutamic acid)-4,7,10-triacetic acid). In an initial study in patients with mCRPC (25,26), ^{177}Lu -DOTAGA-FFK(Sub-KuE) administration led—in some patients—to a significant reduction in metastatic tumor load. In animal studies, higher metabolic stability and thus improved overall pharmacokinetics of PSMA inhibitors was achieved by substitution of the L-amino acid linker part (FFK) between the inhibitor and the chelator (13). Thus, the present study was focused on the further optimization of this second-generation theranostics tracer concept by exploiting the potential of the peptidic linker unit to enhance the PSMA affinity by increasing the lipophilic interaction of the tracer with the PSMA enzyme (8,27). To this aim, DOTAGA-(I-y)fk (Sub-KuE), termed PSMA I&T (for imaging and therapy; Fig. 1), was developed and evaluated in detail, both in vitro and in vivo. On the basis of the promising preclinical data obtained for ^{68}Ga -/ ^{177}Lu -PSMA I&T and to highlight the potential of ^{68}Ga - and ^{177}Lu -PSMA I&T, initial proof of concept in humans is described.

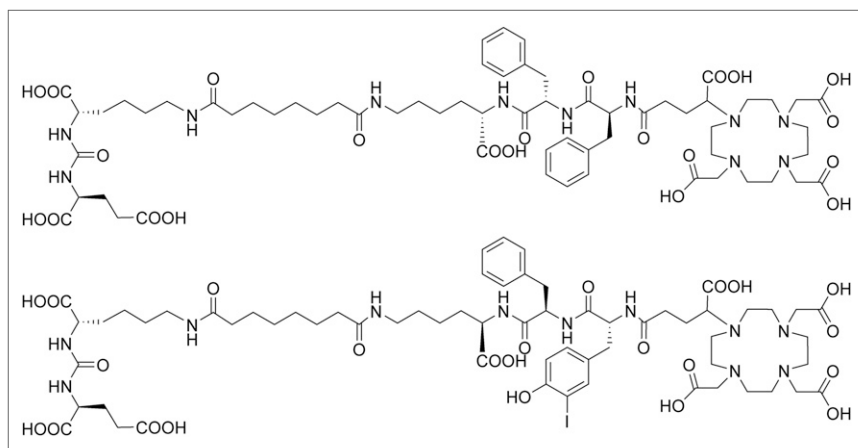


FIGURE 1. Chemical structures of DOTAGA-FFK(Sub-KuE), a first-generation tracer (upper), and PSMA I&T, a third-generation tracer (lower).

MATERIALS AND METHODS

General

All animal experiments were conducted in accordance with the German Animal Welfare Act (Deutsches Tierschutzgesetz, approval no. 55.2-1-54-2532-71-13). All human studies were approved by the institutional review boards of the participating medical institutions. Patients provided signed informed consent.

Synthesis and Radiolabeling

PSMA I&T and its gallium and lutetium complexes were synthesized according to a previously published protocol (13). The synthesis and a detailed description of the ^{68}Ga - and ^{177}Lu -labeling conditions are given in the supplemental data (supplemental materials are available at <http://jnm.snmjournals.org>). The radioiodinated reference ligand ((*S*)-1-carboxy-5-(4-(^{125}I -iodo-benzamido)pentyl)carbamoyl)-L-glutamic acid [^{125}I -BA]KuE) was prepared as described previously (13).

In Vitro Evaluation

The PSMA-positive LNCaP cells (300265; Cell Lines Service GmbH) were grown in Dulbecco modified Eagle medium/Nutrition Mixture F-12 with Glutamax-I (1:1) (Invitrogen) supplemented with 10% fetal calf serum. Cultures were maintained at 37°C in a humidified 5% CO_2 atmosphere. One day before the experiment, cells were harvested using trypsin/ethylenediaminetetraacetate (0.05%/0.02%) in phosphate-buffered saline, centrifuged and resuspended in culture medium, counted, and seeded in 24-well plates.

Determination of PSMA Affinity. The determination of PSMA affinity (IC_{50}) values was performed in a competitive binding assay using LNCaP cells (1.5×10^5 cells in 1 mL/well) and (^{125}I -BA)KuE as radioligand as described previously (13). Quantification of the amount of free and bound activity was performed in a γ counter (Wallac 1480 WIZARD TM 3"; Perkin Elmer, Inc.). IC_{50} values were calculated using PRISM 6 software (GraphPad Software).

Cell Binding Kinetics. Cell binding and internalization kinetics were determined as reported (13). In brief, 1.25×10^5 LNCaP cells in poly-L-lysine-coated 24-well plates were incubated with radiolabeled PSMA I&T (0.2 nM for ^{68}Ga - and 0.5 nM for ^{177}Lu -labeled ligands) at 37°C for 5, 15, 30, and 60 min. The tracers were also incubated in the presence of 10 μM 2-(phosphonomethyl)pentane-1,5-dioic acid (PMPA) solution (blocking), and parallel experiments using the external reference ligand (^{125}I -BA)KuE (0.2 nM) were performed. The amount of radioactivity in the supernatant, PSMA-specifically surface bound (incubation in 250 μL 10 μM PMPA for 10 min at 4°C), and in the cells (lysed with 250 μL 1 M NaOH) was quantified in a γ counter.

In Vivo Evaluation

Animal Model. To induce tumor growth, LNCaP cells ($\sim 10^7$ cells/200 μL) were suspended 1/1 in Dulbecco modified Eagle medium/Nutrition Mixture F-12 with Glutamax-I (1:1) and Matrigel (BD Biosciences) and were inoculated subcutaneously onto the right shoulder of CD-1 *nu/nu* mice (6–8 wk; Charles River Laboratories). After 2–4 wk (males) and 4–6 wk (females), respectively, tumors had reached 4–8 mm in diameter, and the animals were used for experiments.

Dual-Tracer Biodistribution Studies. Both ^{68}Ga -PSMA I&T (4.7–6.3 MBq) and ^{177}Lu -PSMA I&T (1.7–2.0 MBq) were coinjected into the tail vein of LNCaP tumor-bearing male mice under isoflurane anesthesia. The total injected peptide amount was kept constant at 0.2 nmol in all experiments. At 1 h

after injection, the mice were sacrificed, the organs of interest were dissected, and the activity in weighed tissue samples was immediately quantified (^{68}Ga). After the decay of ^{68}Ga (next day), the quantification of ^{177}Lu was performed in a γ counter.

Small-Animal PET Imaging. Imaging studies were performed on a Siemens Inveon small-animal PET scanner. For data analysis the Inveon Research Workplace software was used. Into the tail vein of female animals under isoflurane anesthesia, 14–18 MBq (0.2 nmol) of ^{68}Ga -PSMA I&T were injected. Dynamic imaging was performed for 1.5 h after on-bed injection. Static images were recorded at 1 h after injection with an acquisition time of 15 min. Images were reconstructed using 3-dimensional ordered-subsets expectation maximum algorithm without scanner and attenuation correction.

Dosimetry Calculation

Female wild-type CD-1 mice were injected with 1.3–1.5 MBq of ^{177}Lu -PSMA I&T (33.6–38.7 pmol) and sacrificed at 1, 6, 12, 24, 48, and 96 h after injection ($n = 5$, respectively). Organs of interest were dissected, and the activity in weighed tissue samples was quantified in a γ counter. Using the uptake data at different time points, we performed an extrapolation of the absorbed doses to humans. The dose extrapolation to humans involved the scaling of the time-integrated activity coefficients and the subsequent calculation of the absorbed doses from the animal biodistribution data using 2 different methods. Time-integrated activity coefficients were calculated using the software solution NUKFIT (28). The dose calculation was performed for a selected group of organs using OLINDA/EXM (version 1.1) (29). Details on the methodology used for extrapolating the mouse data to humans are provided in the supplemental data.

^{68}Ga -PSMA I&T PET Imaging in Patients

The patient underwent PET/CT imaging (Biograph mCT PET/CT; Siemens Medical Solution AG) 60 min after intravenous administration of 133.2 MBq of ^{68}Ga -PSMA I&T. CT and reconstruction details are given in the supplemental materials. Circular regions of interest were drawn around areas with increased uptake in transaxial slices for calculation of the maximum standardized uptake value (SUV_{max}). Regions of interest were automatically adapted to a 3-dimensional volume of interest with Syngovia (Siemens Medical Solutions) at a 40% isocontour.

Patient 1, 70 y of age, was diagnosed with PC in 2011, with an initial Gleason score of 10 (5 + 5). The patient had initially undergone palliative transurethral resection of the prostate, followed by androgen-deprivation therapy using abiraterone acetate. Further treatment with docetaxel plus prednisolone was initiated after development of mCRPC, with multiple bone metastases displayed by bone scan. The serum total prostate-specific antigen (PSA) level at the time of imaging was 10.1 ng/mL.

Endoradiotherapy of Patients Using ^{177}Lu -PSMA I&T

Two patients with mCRPC were assessed before the ^{177}Lu -PSMA I&T therapy by ^{68}Ga -PSMA-HBED-CC PET/CT imaging (Biograph mCT Flow 64; Siemens Medical Solutions AG). Contrast-enhanced PET/CT was performed 1–5 d before endoradiotherapy and for follow-up at 65 ± 4 min after intravenous administration of 170 ± 23 MBq of ^{68}Ga -PSMA-HBED-CC. Both patients with progressive mCRPC underwent therapy with 5.7 and 8.0 GBq of ^{177}Lu -PSMA I&T, respectively, administered intravenously over 15 min. Complete blood counts, parameters of renal function (serum creatinine, blood urea nitrogen), and liver function (albumin, bilirubin, enzymes), as well as tubular extraction rate measured by $^{99\text{m}}\text{Tc}$ -mercaptoacetyltryglycine scintigraphy, were documented before and after therapy. Response to therapy was assessed by ^{68}Ga -PSMA-HBED-CC PET combined with contrast-enhanced CT 8–10 wk after therapy. In addition, biochemical response was documented by means of PSA monitoring.

Patient 2 was a 68-y-old man with progressive metastatic prostatic adenocarcinoma (Gleason score 7) and multiple mediastinal lymph node metastases. The 54-y-old patient 3, with adenocarcinoma-of-the-prostate (Gleason score 9: 4 + 5) status after hormonal therapy and external-beam radiation therapy, presented with progressive mediastinal and retroperitoneal lymph node metastases and multifocal osseous lesions.

RESULTS

Synthesis and Radiolabeling

PSMA I&T was synthesized in accordance with the protocol described for DOTAGA-ffk(Sub-KuE) (13) and obtained in 32.4% yield (based on DOTAGA-(I-y)fk) and greater than 99% purity (220 nm).

For cell studies, manual ^{68}Ga labeling of PSMA I&T (3 nmol) resulted in a specific activity of 250–300 GBq/ μmol , whereas for animal studies fully automated ^{68}Ga labeling (5 nmol) yielded ^{68}Ga -PSMA I&T in specific activities of 80–120 GBq/ μmol . For quantitative ^{177}Lu complexation, 24.5 MBq of $^{177}\text{Lu}^{\text{III}}$ was reacted with a 4.5-fold molar excess of PSMA I&T, yielding ^{177}Lu -PSMA I&T in specific activities of 27 GBq/ μmol or more.

Tracers for patient application were prepared using a fully automated synthesis module and obtained in radiochemical yields of $67\% \pm 10\%$ (non-decay-corrected) and radiochemical purities of $98\% \pm 2\%$ (instant thin-layer chromatography silica gel; Varian). Calculated specific activities were 40.0 MBq/ μg (37.8 GBq/ μmol) for ^{68}Ga -PSMA-HBED-CC and 13.6 MBq/ μg (20.4 GBq/ μmol) for ^{68}Ga -PSMA I&T. For ^{177}Lu -PSMA I&T, the radiochemical purity was $99.0\% \pm 1.0\%$ as determined by reversed-phase high-performance liquid chromatography (LiChroCART 250-4, Lichrospher100, RP18; Merck), and specific activities of 40.0 MBq/ μg (59.9 GBq/ μmol) were achieved.

PSMA Binding Affinity

The affinity (IC_{50}) of PSMA I&T and its $^{\text{nat}}\text{Ga}$ and $^{\text{nat}}\text{Lu}$ complexes toward PSMA (Table 1) was determined in a competitive binding assay using the human prostate carcinoma cell line LNCaP (1.5×10^5 cells/well, 1 h) at 4°C and (^{125}I -BA)KuE (0.2 nM) as the radioligand.

Compared with the second-generation DOTAGA-functionalized PSMA ligands (13), PSMA I&T contains a D-Phe-by-3-iodo-D-Tyr substitution in the peptidic linker unit (Fig. 1). To be able to assess the influence of this modification on PSMA affinity, data for DOTAGA-ffk(Sub-KuE) (13) are also included in Table 1. Metal

TABLE 1

IC_{50} Values Determined in Competitive Binding Assay

Ligand	IC_{50} (nM)
DOTAGA-ffk(Sub-KuE)	13.9 ± 0.4
$^{\text{nat}}\text{Ga}$ -DOTAGA-ffk(Sub-KuE)	15.9 ± 0.5
$^{\text{nat}}\text{Lu}$ -DOTAGA-ffk(Sub-KuE)	13.1 ± 2.2
PSMA I&T (DOTAGA-(I-y)fk(Sub-KuE))	10.2 ± 3.5
$^{\text{nat}}\text{Ga}$ -PSMA I&T	9.3 ± 3.3
$^{\text{nat}}\text{Lu}$ -PSMA I&T	7.9 ± 2.4

(LNCaP, $c(^{125}\text{I}\text{-BA})\text{KuE} = 0.2$ nM, Hank's balanced salt solution + 1% bovine serum albumin, 1 H, 4°C). Data are expressed as mean \pm SD ($n = 3$ in 3 separate determinations).

complexation has only negligible effect on PSMA affinity of PSMA I&T. However, substitution of D-Phe by D-3-iodo-Tyr in the linker does have beneficiary influence in significantly improving PSMA affinity of the PSMA I&T constructs as compared with the second-generation DOTAGA analogs.

Internalization Kinetics

To investigate the impact of the increased affinity of ^{68}Ga -/ ^{177}Lu -PSMA I&T on ligand internalization and cell binding, LNCaP cells (1.25×10^5 cells/well) were incubated with the respective radioligands at 37°C for different time points up to 1 h. Experiments were performed in the absence (total binding) and presence of 10 μM PMPA (nonspecific binding), and a PMPA wash step (10 μM , 10 min, 4°C) was included to differentiate between specifically bound and internalized activity. To exclude an influence of interexperimental variations in cell count or cell viability on the absolute amount of bound/internalized tracer, the standard ligand (^{125}I -BA)KuE was always assayed in parallel as an external reference, and its cellular uptake in the respective experiments was used for data normalization.

The upper portion of Figure 2 shows the ligand binding kinetics of ^{177}Lu -PSMA I&T in comparison to ^{177}Lu -DOTAGA-ffk(Sub-KuE). The internalization of all ^{68}Ga - and ^{177}Lu -labeled PSMA inhibitors investigated in this study was high and nearly identical. At all time points, 1%–3% of the total activity was bound to PSMA on the cell membrane (Fig. 2 [lower]), and less than 0.5% was nonspecifically bound. Although ^{177}Lu -DOTAGA-ffk(Sub-KuE) showed only 44% \pm 2% of the cellular uptake of the reference compound (^{125}I -BA)KuE in a parallel experiment, internalization of ^{177}Lu -PSMA I&T was increased to 76% \pm 2% of that of (^{125}I -BA)KuE. The same trend was observed for the respective ^{68}Ga -labeled analogs, for which the transition from ^{68}Ga -DOTAGA-ffk(Sub-KuE) to ^{68}Ga -PSMA I&T led to an increase in internalization from 42% \pm 2% to 59% \pm 2% of (^{125}I -BA)KuE internalization.

Dual-Tracer Biodistribution Study

The biodistribution of ^{68}Ga -PSMA I&T (0.1 nmol) and ^{177}Lu -PSMA I&T (0.1 nmol) investigated in a dual-tracer experiment at 1 h after injection in LNCaP tumor-bearing CD-1 *nu/nu* mice is summarized in Table 2. Given their nearly identical physicochemical properties, both ^{68}Ga - and ^{177}Lu -PSMA I&T showed fast and rapid clearance from the circulation and virtually no background accumulation at 1 h after injection (Table 2). Interestingly, the increased PSMA-mediated internalization of ^{177}Lu -PSMA I&T, compared with its ^{68}Ga analog, was well reflected by an enhanced uptake in the PSMA-positive tissues—that is, lung, spleen, and a significantly ($P < 0.05$) higher kidney and tumor uptake. Therefore, tumor-to-background ratios for ^{177}Lu -PSMA I&T are increased for almost all organs (Fig. 3).

Small-Animal PET Imaging

As shown on the PET images of LNCaP tumor-bearing CD-1 *nu/nu* mice at 1 h after injection, ^{68}Ga -PSMA I&T primarily accumulates in the tumor xenograft and the kidneys, which were shown to be PSMA-specific (Fig. 4A). Fast renal excretion was confirmed by significant bladder activity. The time-activity curves (Fig. 4B) derived from dynamic PET data revealed fast uptake kinetics and retention of the tracer in kidney and tumor over the 1.5-h observation period, whereas the activity was rapidly washed out from nontarget tissues and compartments such as blood (region of interest over the heart) and muscle (linear decline in a logarithmic plot).

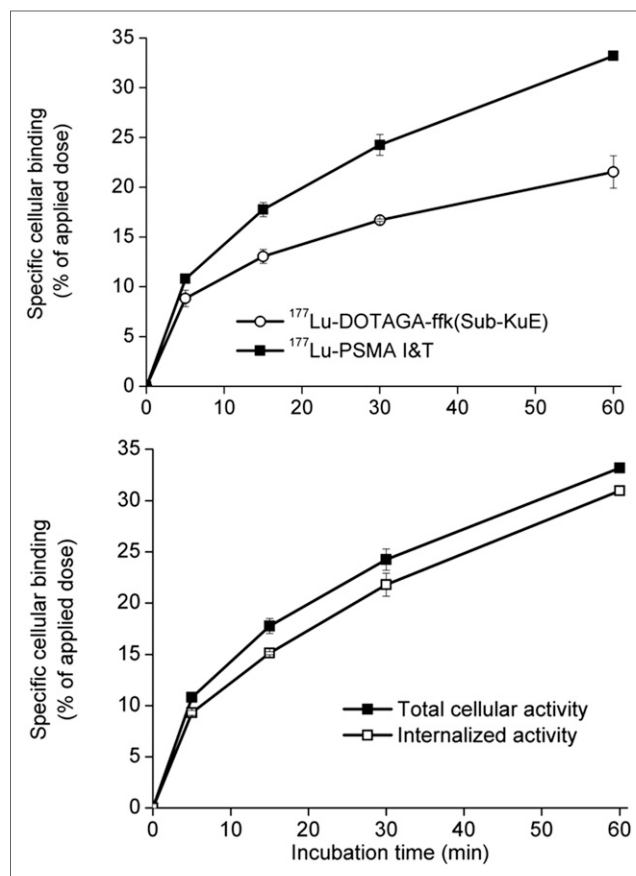


FIGURE 2. Specific binding kinetics of ^{177}Lu -PSMA I&T and ^{177}Lu -DOTAGA-ffk(Sub-KuE) (upper) and specific binding and internalization kinetics of ^{177}Lu -PSMA I&T at 37°C to LNCaP cells (lower). All data are expressed as mean \pm SD.

TABLE 2
Dual-Tracer Biodistribution (%ID/g) in LNCaP Tumor-Bearing CD-1 *nu/nu* Mice at 1 Hour After Injection ($n = 4$)

Organ	^{68}Ga -PSMA I&T	^{177}Lu -PSMA I&T
Blood	0.45 \pm 0.23	0.44 \pm 0.19
Heart	0.26 \pm 0.08	0.29 \pm 0.08
Lung	1.49 \pm 0.38	1.65 \pm 0.56
Liver	1.00 \pm 0.39	1.10 \pm 0.41
Spleen	3.88 \pm 1.46	5.85 \pm 2.26
Pancreas	0.54 \pm 0.15	0.57 \pm 0.24
Stomach	0.42 \pm 0.10	0.42 \pm 0.14
Intestine	0.27 \pm 0.07	0.69 \pm 0.14
Kidney	53.26 \pm 9.02	107.24 \pm 15.61
Muscle	0.35 \pm 0.08	0.56 \pm 0.36
Brain	0.03 \pm 0.02	0.04 \pm 0.03
Bone	0.27 \pm 0.08	0.22 \pm 0.05
Tumor	4.95 \pm 1.57	7.96 \pm 1.76

%ID/g = percentage injected dose per gram.

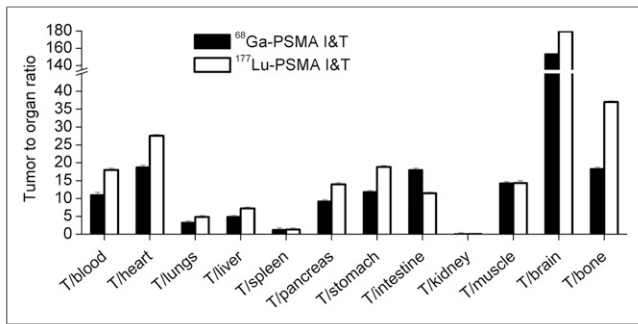


FIGURE 3. Tumor-to-organ ratios of dual-tracer biodistribution of ^{68}Ga - and ^{177}Lu -PSMA I&T at 1 h after injection in LNCaP tumor-bearing CD-1 *nu/nu* mice ($n = 4$). T/ = tumor-to-.

Dosimetry of ^{177}Lu -PSMA I&T in Mice

Absorbed doses for ^{177}Lu -PSMA I&T in humans were extrapolated from mouse biodistribution data using 2 alternative extrapolation methods (method 1 [M1] and method 2 [M2]). Details on the methodology, a list of the time-integrated activity coefficients for several organs of relevance for dosimetry (residence times), a full list of the corresponding absorbed doses, and information on the absorbed dose by β particles and photons are given in the supplemental data. The highest time-integrated activity coefficient was observed for the kidneys (M1, 8.3 h; M2, 5.8 h). For all organs, the total absorbed doses are summarized in Table 3 and were lower than 5.9×10^{-2} mGy/MBq (adrenals M1), except kidneys (2.4 mGy/MBq [M1] or 1.6 mGy/MBq [M2]). Unless more than 9.6 GBq (M1) or 14.4 GBq (M2) are administered to humans, the limiting kidney dose of 23 Gy could be exceeded.

In addition, the effective dose per unit activity in kidneys was calculated. However, the quantity effective dose can be applied only to the description of stochastic radiation effects and organ-absorbed doses of less than 1 Gy. The extrapolated effective doses were 9.6×10^{-3} mSv/MBq (M1) and 7.4×10^{-3} mSv/MBq (M2), which corresponded to effective doses of 1.9 mSv (M1) and 1.5 mSv (M2) for an administered activity of 200 MBq.

^{68}Ga -PSMA I&T PET Imaging in First Patient

In a first patient with CRPC with multiple metastases ^{68}Ga -PSMA I&T PET/CT revealed multiple bone, abdominal lymph node, and a liver metastasis (Fig. 5A). The primary prostate tumor

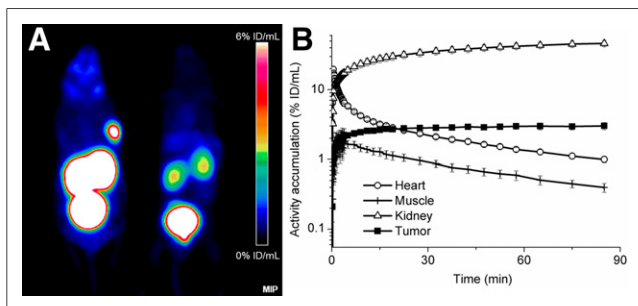


FIGURE 4. PET of LNCaP tumor-bearing CD-1 *nu/nu* mice. (A) Maximum-intensity projections (MIP) of static PET scans using 15.8 MBq of ^{68}Ga -PSMA I&T (left) or 14.3 MBq of ^{68}Ga -PSMA I&T coinjected with PMPA (8 mg/kg) (right). (B) Time-activity curves (logarithmic plot) for ^{68}Ga -PSMA I&T (15.4 MBq) derived from dynamic small-animal PET data. ID = injected dose.

TABLE 3

Total Absorbed Doses in Different Organs (mGy/MBq) after Application of ^{177}Lu -PSMA I&T, Calculated by Both Methods

Target organ	Total absorbed dose (mGy/MBq)	
	M1	M2
Adrenals	5.85E-02	4.10E-02
Brain	5.10E-04	5.91E-04
Breasts	2.50E-04	2.28E-04
Gallbladder wall	3.42E-03	2.43E-03
Lower large intestine wall	5.65E-04	4.40E-04
Small intestine	9.25E-03	2.64E-03
Stomach wall	5.56E-03	2.60E-03
Upper large intestine wall	1.92E-03	1.34E-03
Heart wall	1.86E-03	1.91E-03
Kidneys	2.40E+00	1.66E+00
Liver	6.56E-03	5.10E-03
Lung	7.81E-03	1.22E-02
Muscle	9.04E-04	1.93E-03
Ovaries	7.36E-04	5.33E-04
Pancreas	1.79E-02	5.75E-03
Red marrow	2.00E-03	1.99E-03
Osteogenic cells	4.83E-03	8.45E-03
Skin	3.92E-04	3.17E-04
Spleen	3.07E-02	1.95E-02
Testes	8.18E-05	1.16E-04
Thymus	2.42E-04	2.58E-04
Thyroid	9.28E-05	1.42E-04
Urinary bladder wall	2.73E-04	2.39E-04
Uterus	3.33E-02	5.90E-03
Total body	1.12E-02	8.45E-03

Details on M1 and M2 are provided in supplemental data.

(SUV_{max} , 65.1; Fig. 5B), as well as periprostatic tissue and urinary bladder invasion, was not concealed by radioactivity in the bladder. A 7-mm left perirectal lymph node showed an SUV_{max} of 15. The liver lesion (Fig. 5C), which was not known before PET scanning, showed an SUV_{max} of 10.9 and 2 cm in diameter. Further, a sclerosis in a sternal lesion, which had been barely visible in the CT image, exhibited a high ^{68}Ga -PSMA I&T uptake (SUV_{max} , 76.4; Fig. 5E). Multiple paraaortic and pelvic lymph nodes showed high contrast in ^{68}Ga -PSMA I&T PET, as shown for an 8-mm paraaortic lymph node with an SUV_{max} of 39.4 in Figure 5D. Mean SUV_{max} of lymph node metastases was 26.4 (range, 7–80.4) and of bone metastases 52.8 (range, 22–76.5). The average ^{68}Ga -PSMA I&T lesion-to-background ratio was 17.6 for lymph node metastases, 35.2 for bone metastases, and 20.7 for the liver metastasis. Background activity was determined in gluteal musculature (SUV_{max} , 1.5).

Besides the pathologic tracer accumulation, ^{68}Ga -PSMA I&T showed a high uptake in the kidneys and salivary glands and low

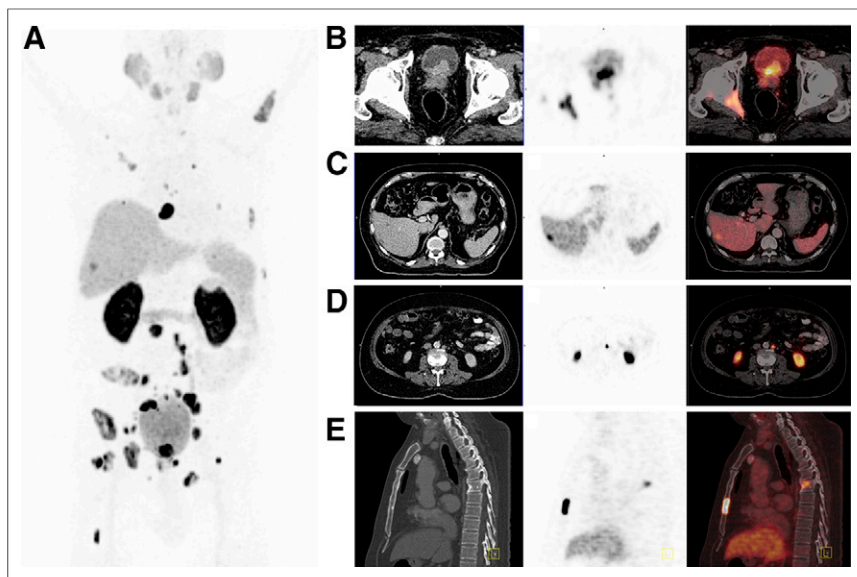


FIGURE 5. ^{68}Ga -PSMA I&T PET/CT of patient 1. (A) Whole-body maximum-intensity projection showing 1 liver lesion and multiple lymph node and bone metastases. (B) Transaxial slices show infiltration of soft-tissue mass with increased tracer uptake in urinary bladder and periprostatic tissue. (C) Transaxial slices revealing ^{68}Ga -PSMA I&T uptake in right lobe of liver with hypodense lesion in corresponding CT slice. (D) Transaxial slices presenting small paraaortic lymph node with intense PSMA expression indicative of lymph node metastasis. (E) Sagittal reformatted CT reveals only minimal sclerosis of sternal bone metastasis with high ^{68}Ga -PSMA I&T uptake. All slices are shown on CT (left), PET (middle), and fused PET/CT (right).

uptake in the liver, spleen, and proximal segments of the small intestine.

^{177}Lu -PSMA I&T Therapy in Patients

Two patients with mCRPC and multiple metastases in bone and lymph nodes, which had been confirmed by baseline ^{68}Ga -PSMA-HBED-CC PET/CT, were treated with ^{177}Lu -PSMA I&T. Therapy control was performed using ^{68}Ga -PSMA-HBED-CC PET/CT to ensure comparability to data from the literature and an objective interpretation of the therapy outcome. The administered mass of PSMA I&T was 142 and 200 μg , and the administered activity was 5.7 and 8.0 GBq, respectively. In patient 2 (PSA, 54.2 ng/mL), the mediastinal lymph node metastases (SUV_{max} , 36.5, determined by ^{68}Ga -PSMA-HBED-CC PET/CT) exhibited a high uptake of ^{177}Lu -PSMA I&T (Fig. 6) on posttherapy planar and SPECT/CT images. Therapy was well tolerated, and no significant fall in blood counts, renal function (serum creatinine, tubular extraction rate), or any of the laboratory parameters was found. There was no adverse or clinically detectable pharmacologic effect. During early follow-up, no side effects were observed, particularly no dry mouth caused by activity in salivary glands.

The baseline ^{68}Ga -PSMA-HBED-CC PET/CT scan in patient 3 (PSA, 40.2 ng/mL) demonstrated PSMA-mediated uptake in the primary tumor and multiple lymph node and bone metastases (Fig. 7A). The SUV_{max} of target lesions was 26.3 in the right paraaortic lymph node (transverse PET/CT image in Fig. 7A, upper), 25.2 in interaortocaval lymph node (Fig. 7A, middle), and 16.4 in the primary tumor in the prostate (Fig. 7A, lower). The patient underwent 1 therapy cycle with 8.0 GBq of ^{177}Lu -PSMA I&T. Follow-up ^{68}Ga -PSMA-HBED-CC PET/CT (Fig. 7B) 3 mo after ^{177}Lu -PSMA I&T therapy revealed partial remission of many of the intense PSMA-positive metastases depicted by ^{68}Ga -PSMA-HBED-CC PET/CT (SUV_{max} , 3.0, 3.5, and 5.1 in paraaortic,

interaortocaval lymph node metastasis, and primary tumor, respectively) accompanied by a significant drop in the PSA to 0.7 ng/mL. Clinically, a symptomatic pain relief, especially on the left side of the chest, was reported.

DISCUSSION

In comparison to ^{18}F -fluoromethylcholine, the urea-based PSMA inhibitor ^{68}Ga -PSMA-HBED-CC (30) displays significantly improved diagnostic sensitivity and specificity. To meet the urgent need for a targeted therapeutic agent in the treatment of PC, first promising (urea-based) candidates for endoradiotherapy of PC have also been introduced and evaluated in first patient studies (25,26,31).

On the basis of the valuable results of this tracer class both in diagnostic imaging and in endoradiotherapy, the aim of this study was the development of a suitable PSMA-targeted theranostic concept, combining straightforward labeling procedures for clinical routine application with optimized PSMA-targeting characteristics. Previous studies leading to a first-generation theranostic agent (Fig. 1) have already

demonstrated the beneficial effect of DOTAGA-for-DOTA substitution and of using an all-D-amino acid peptide linker on PSMA affinity and metabolic stability and thus uptake and clearance kinetics, respectively (13). Complementing these findings with the substitution of 1 of the D-phenylalanine residues in the peptidic linker by 3-iodo-D-tyrosine for an improved interaction of the tracer molecule with a remote binding site (27) led to PSMA I&T (Fig. 1). As anticipated, this modification resulted in an increased PSMA affinity of PSMA I&T and its $^{\text{nat}}\text{Ga}$ and $^{\text{nat}}\text{Lu}$ complexes, compared with their ffk analogs (Table 1), which is

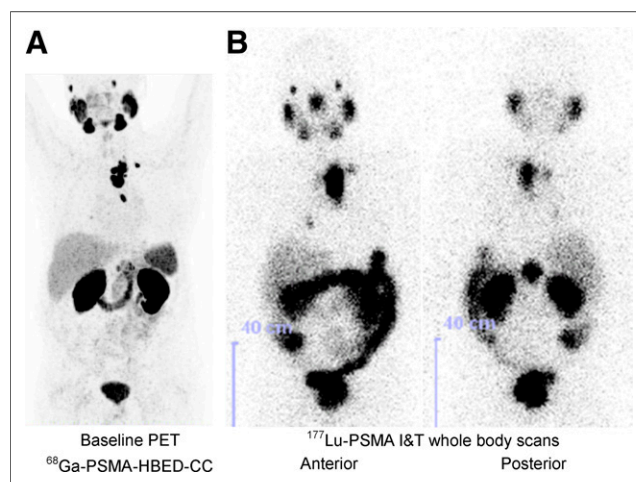


FIGURE 6. Patient 2. (A) Maximum-intensity projection of ^{68}Ga -PSMA-HBED-CC PET/CT (164 MBq, 60 min after injection, left) showed intense tracer accumulation in mediastinal lymph node metastases. (B) Correspondingly, these mediastinal lymph nodes demonstrated high ^{177}Lu -PSMA I&T uptake 47 h after therapy with 5.7 GBq of ^{177}Lu -PSMA I&T.

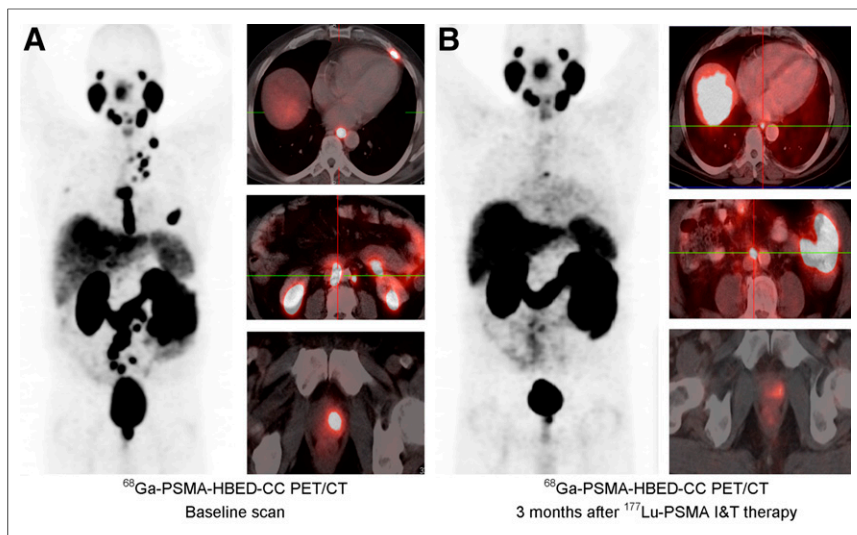


FIGURE 7. PET/CT in patient 3. (A) Baseline PET/CT 65 min after intravenous administration of 176 MBq of ^{68}Ga -PSMA-HBED-CC. (B) Follow-up scan with 180 MBq of ^{68}Ga -PSMA-HBED-CC (60 min after injection) performed 3 mo after ^{177}Lu -PSMA I&T therapy (8.0 GBq).

also reflected by an enhanced internalization efficiency of ^{68}Ga -/ ^{177}Lu -PSMA I&T into PSMA-expressing LNCaP cells. Interestingly, although the PSMA affinity of ^{nat}Lu -PSMA I&T is only marginally increased, compared with ^{nat}Ga -PSMA I&T, internalization of ^{177}Lu -PSMA I&T into LNCaP cells is significantly enhanced. This improved targeting efficiency is reflected by an increased uptake of ^{177}Lu -PSMA I&T in the LNCaP tumor xenografts and thus enhanced tumor-to-background ratios (Fig. 3). It also shows a nearly 2-fold-higher accumulation in lung, spleen, and kidney, all of which are tissues with documented PSMA expression (32). Compared with other promising PSMA-directed tracers, ^{68}Ga - and ^{177}Lu -PSMA I&T both show a tissue distribution pattern comparable to that of ^{68}Ga -PSMA-HBED-CC (11,13) at the same time point. Although both compounds show enhanced blood activity levels and liver accumulation, compared with ^{99m}Tc -MIP-1404 (12), the extent of PSMA-unspecific activity retention in the blood and liver was significantly lower than ^{18}F -DCFBC (7). This difference in retention is most probably the result of the excellent metabolic stability and comparably low plasma protein binding of ^{68}Ga -/ ^{177}Lu -PSMA I&T.

First clinical application of ^{68}Ga -PSMA I&T in PET/CT successfully demonstrated multiple metastatic foci in different organs and tissues with high lesion-to-background ratios of 17.6–35.2 as early as 1 h after injection. Even very small (millimeter range) abdominal lymph node and small bone metastases showed high uptake and were easily detectable (Fig. 5). Comparable to previously reported data for ^{68}Ga -PSMA-HBED-CC in PET/CT (14), low physiologic tracer uptake was observed in the liver (33), spleen (33), and intestine (3) and—to a higher extent—in the proximal tubules of the kidneys (3) and salivary glands (34), all of which are organs with documented moderate to high PSMA expression. However, the reasons for the observed high tracer uptake into salivary glands is still a matter of debate, because the PSMA expression level would suggest lower uptake.

Because there is presently no standardized way for extrapolating time-integrated activity coefficients from animal data to humans, we decided to apply 2 methods originally described by Sparks and Aydogan (35). Choosing 2 different ways of scaling

provides an estimate of the extrapolation-related uncertainty in calculating absorbed doses to humans, as can be seen in Table 3. Overall, the agreement between the absorbed doses to the organs is acceptable. For most organs, the difference is less than $\pm 45\%$. Major deviations caused by the different ways of extrapolating are for the intestines, pancreas, and uterus. If, for therapeutic applications, organs at risk need to be considered for a first-in-human study, one would apply the higher of both values as a conservative estimate of the organ-absorbed doses.

The extrapolated organ dosimetry for ^{177}Lu -PSMA I&T shows that the highest absorbed dose per unit activity is expected in the kidneys. The values are about 1.1- to 1.7-fold higher than the corresponding values reported for ^{131}I -MIP-1095 with 1.5 mGy/MBq (31) and for ^{177}Lu -J591 with 1.4 mGy/MBq (23). For ^{90}Y -J591 (23), a value of 4.5 mGy/MBq is reported, which is

about 2 times higher than the extrapolated values for ^{177}Lu -PSMA I&T. In addition, the calculated absorbed doses per unit activity for other organs (e.g., liver, spleen, heart wall, bone marrow) for ^{131}I -MIP-1095 (31) and ^{177}Lu -J591 (23) are at least 1 order of magnitude higher than the corresponding values for ^{177}Lu -PSMA I&T. Of course the present extrapolated data need to be confirmed in a dosimetry study in patients, including an assessment of the absorbed doses to tumor lesions in patients.

As its ^{68}Ga analog, ^{177}Lu -PSMA I&T shows high, specific and rapid uptake in all previously identified tumor lesions of the mCRPC patients included in this proof-of-concept study (Fig. 6). As expected, significant tracer uptake is also observed for the kidney, spleen, and salivary glands but also in the small intestine. This finding is consistent with the PSMA expression levels documented for these tissues (3,33,34); for example, ^{177}Lu -PSMA I&T uptake in the small intestine most likely is the result of PSMA expression in human intestine (3), in which the physiologic function of PSMA is mediating folate absorption (36). On the basis of the high PSMA expression in the metastases of mCRPC (37) and the resulting high uptake of ^{177}Lu -PSMA I&T in these lesions, therapeutically effective doses were delivered to the PC metastases resulting in impressive molecular treatment response. Besides concomitant subjective reduction of pain, both patients demonstrated objective clinical measures of improvement, such as a drop of PSA and reduction of disease burden as determined by ^{68}Ga -PSMA-HBED-CC PET/CT (Fig. 7).

Because of the rapid renal washout and blood clearance of ^{177}Lu -PSMA I&T, no side effects either in salivary glands or in kidneys or blood parameters were observed in either of the 2 treated patients, and treatment was well tolerated. In contrast, after endoradiotherapy with ^{131}I -MIP-1095 (31) dry mouth and 1 case of mucositis were reported due to high salivary gland retention of the therapeutic agent. Thus, high contrast in PET imaging and therapeutic effectiveness with no detectable side effects qualifies ^{68}Ga -/ ^{177}Lu -PSMA I&T to be a valid choice for the theranostic management of PC.

CONCLUSION

⁶⁸Ga-PSMA I&T is a PET tracer of high potential for the detection of metastatic PC and may be useful for stratification and follow-up of patients undergoing radioligand therapy with ¹⁷⁷Lu-PSMA I&T (theranostics). In a proof-of-concept study ¹⁷⁷Lu-PSMA I&T endoradiotherapy was feasible, safe, and effective in metastatic PC. Subsequent studies have to assess the optimal activity as well as the amount of peptide administered, potential kidney or salivary gland protection, and the need of repeated therapeutic interventions based on patient follow-up.

DISCLOSURE

The costs of publication of this article were defrayed in part by the payment of page charges. Therefore, and solely to indicate this fact, this article is hereby marked "advertisement" in accordance with 18 USC section 1734. The research leading to these results has received funding from the Deutsche Forschungsgemeinschaft (DFG) under grant agreement no. SFB 824 project Z1. Jakub Simecek is an employee and Hans-Jürgen Wester is CEO of SCINTOMICS GmbH, Fuerstenfeldbruck, Germany. No other potential conflict of interest relevant to this article was reported.

ACKNOWLEDGMENTS

We thank Frauke Hoffmann and Simon Schmiel for experimental assistance and Sybille Reder, Markus Mittelhäuser, and Marco Lehmann for small-animal PET imaging.

REFERENCES

1. Reubi JC, Schar JC, Waser B, et al. Affinity profiles for human somatostatin receptor subtypes SST1-SST5 of somatostatin radiotracers selected for scintigraphic and radiotherapeutic use. *Eur J Nucl Med*. 2000;27:273–282.
2. Reubi JC, Laissue J, Krenning E, Lamberts SW. Somatostatin receptors in human cancer: incidence, characteristics, functional correlates and clinical implications. *J Steroid Biochem Mol Biol*. 1992;43:27–35.
3. Silver DA, Pellicer I, Fair WR, Heston WD, Cordon-Cardo C. Prostate-specific membrane antigen expression in normal and malignant human tissues. *Clin Cancer Res*. 1997;3:81–85.
4. Sweat SD, Pacelli A, Murphy GP, Bostwick DG. Prostate-specific membrane antigen expression is greatest in prostate adenocarcinoma and lymph node metastases. *Urology*. 1998;52:637–640.
5. Pomper MG, Musachio JL, Zhang J, et al. ¹¹C-MCG: synthesis, uptake selectivity, and primate PET of a probe for glutamate carboxypeptidase II (NAALADase). *Mol Imaging*. 2002;1:96–101.
6. Foss CA, Mease RC, Fan H, et al. Radiolabeled small-molecule ligands for prostate-specific membrane antigen: in vivo imaging in experimental models of prostate cancer. *Clin Cancer Res*. 2005;11:4022–4028.
7. Mease RC, Dusich CL, Foss CA, et al. *N*-[*N*-(*S*)-1,3-dicarboxypropyl]carbamoyl]-4-[¹⁸F]fluorobenzyl-L-cysteine, [¹⁸F]DCFBC: a new imaging probe for prostate cancer. *Clin Cancer Res*. 2008;14:3036–3043.
8. Kularatne SA, Zhou Z, Yang J, Post CB, Low PS. Design, synthesis, and preclinical evaluation of prostate-specific membrane antigen targeted ^{99m}Tc-radioimaging agents. *Mol Pharm*. 2009;6:790–800.
9. Hillier SM, Maresca KP, Femia FJ, et al. Preclinical evaluation of novel glutamate-urea-lysine analogues that target prostate-specific membrane antigen as molecular imaging pharmaceuticals for prostate cancer. *Cancer Res*. 2009;69:6932–6940.
10. Banerjee SR, Pullambhatla M, Byun Y, et al. ⁶⁸Ga-labeled inhibitors of prostate-specific membrane antigen (PSMA) for imaging prostate cancer. *J Med Chem*. 2010;53:5333–5341.
11. Eder M, Schafer M, Bauder-Wust U, et al. ⁶⁸Ga-complex lipophilicity and the targeting property of a urea-based PSMA inhibitor for PET imaging. *Bioconjug Chem*. 2012;23:688–697.
12. Hillier SM, Maresca KP, Lu G, et al. ^{99m}Tc-labeled small-molecule inhibitors of prostate-specific membrane antigen for molecular imaging of prostate cancer. *J Nucl Med*. 2013;54:1369–1376.

13. Weineisen M, Simecek J, Schottelius M, Schwaiger M, Wester H-J. Synthesis and preclinical evaluation of DOTAGA-conjugated PSMA ligands for functional imaging and endoradiotherapy of prostate cancer. *EJNMMI Research*. 2014;4:63.
14. Afshar-Oromieh A, Malcher A, Eder M, et al. PET imaging with a [⁶⁸Ga] gallium-labelled PSMA ligand for the diagnosis of prostate cancer: biodistribution in humans and first evaluation of tumour lesions. *Eur J Nucl Med Mol Imaging*. 2013;40:486–495.
15. Barrett JA, Coleman RE, Goldsmith SJ, et al. First-in-man evaluation of 2 high-affinity PSMA-avid small molecules for imaging prostate cancer. *J Nucl Med*. 2013;54:380–387.
16. Cho SY, Gage KL, Mease RC, et al. Biodistribution, tumor detection, and radiation dosimetry of ¹⁸F-DCFBC, a low-molecular-weight inhibitor of prostate-specific membrane antigen, in patients with metastatic prostate cancer. *J Nucl Med*. 2012;53:1883–1891.
17. Vallabhajosula S, Nikolopoulou A, Babich JW, et al. ^{99m}Tc-labeled small-molecule inhibitors of prostate-specific membrane antigen: pharmacokinetics and biodistribution studies in healthy subjects and patients with metastatic prostate cancer. *J Nucl Med*. 2014;55:1791–1798.
18. Heidenreich A, Bellmunt J, Bolla M, et al. EAU guidelines on prostate cancer: part 1—screening, diagnosis, and treatment of clinically localised disease. *Eur Urol*. 2011;59:61–71.
19. Sharifi N, Gulley JL, Dahut WL. Androgen deprivation therapy for prostate cancer. *JAMA*. 2005;294:238–244.
20. Parker C, Nilsson S, Heinrich D, et al. Alpha emitter radium-223 and survival in metastatic prostate cancer. *N Engl J Med*. 2013;369:213–223.
21. Sodee DB, Malguria N, Faulhaber P, Resnick MI, Albert J, Bakale G. Multicenter ProstaScint imaging findings in 2154 patients with prostate cancer. The ProstaScint Imaging Centers. *Urology*. 2000;56:988–993.
22. Liu H, Moy P, Kim S, et al. Monoclonal antibodies to the extracellular domain of prostate-specific membrane antigen also react with tumor vascular endothelium. *Cancer Res*. 1997;57:3629–3634.
23. Vallabhajosula S, Goldsmith SJ, Hamacher KA, et al. Prediction of myelotoxicity based on bone marrow radiation-absorbed dose: radioimmunotherapy studies using ⁹⁰Y- and ¹⁷⁷Lu-labeled J591 antibodies specific for prostate-specific membrane antigen. *J Nucl Med*. 2005;46:850–858.
24. Tagawa ST, Milowsky MI, Morris M, et al. Phase II study of lutetium-177-labeled anti-prostate-specific membrane antigen monoclonal antibody J591 for metastatic castration-resistant prostate cancer. *Clin Cancer Res*. 2013;19:5182–5191.
25. Kulkarni H, Weineisen M, Mueller D, et al. First clinical results with Lu-177 PSMA-TUM1 for the treatment of castrate-resistant metastatic prostate cancer [abstract]. *J Nucl Med*. 2014;55(suppl 1):10.
26. Schuchardt C, Weineisen M, Wiessalla S, et al. Biodistribution and dosimetry of Lu-177 PSMA in metastasized castrate resistant prostate cancer patients [abstract]. *J Nucl Med*. 2014;55(suppl 1):641.
27. Zhang AX, Murelli RP, Barinka C, et al. A remote arene-binding site on prostate specific membrane antigen revealed by antibody-recruiting small molecules. *J Am Chem Soc*. 2010;132:12711–12716.
28. Kletting P, Schimmel S, Kestler HA, et al. Molecular radiotherapy: the NUKFIT software for calculating the time-integrated activity coefficient. *Med Phys*. 2013;40:102504.
29. Stabin MG, Sparks RB, Crowe E. OLINDA/EXM: the second-generation personal computer software for internal dose assessment in nuclear medicine. *J Nucl Med*. 2005;46:1023–1027.
30. Afshar-Oromieh A, Zechmann CM, Malcher A, et al. Comparison of PET imaging with a ⁶⁸Ga-labelled PSMA ligand and ¹⁸F-choline-based PET/CT for the diagnosis of recurrent prostate cancer. *Eur J Nucl Med Mol Imaging*. 2014;41:11–20.
31. Zechmann CM, Afshar-Oromieh A, Armor T, et al. Radiation dosimetry and first therapy results with a ¹²⁴I/¹³¹I-labeled small molecule (MIP-1095) targeting PSMA for prostate cancer therapy. *Eur J Nucl Med Mol Imaging*. 2014;41:1280–1292.
32. Eder M, Schafer M, Bauder-Wust U, Haberkorn U, Eisenhut M, Kopka K. Preclinical evaluation of a bispecific low-molecular heterodimer targeting both PSMA and GRPR for improved PET imaging and therapy of prostate cancer. *Prostate*. 2014;74:659–668.
33. O'Keefe DS, Bacich DJ, Heston WD. Comparative analysis of prostate-specific membrane antigen (PSMA) versus a prostate-specific membrane antigen-like gene. *Prostate*. 2004;58:200–210.
34. Israeli RS, Powell CT, Corr JG, Fair WR, Heston WD. Expression of the prostate-specific membrane antigen. *Cancer Res*. 1994;54:1807–1811.
35. Sparks RB, Aydogan B. Comparison of the effectiveness of some common animal data scaling techniques in estimating human radiation dose. In: Stetson A, Stabin M, Sparks R, eds. *Sixth International Radiopharmaceutical Dosimetry Symposium*. Oak Ridge, TN: Oak Ridge Associated Universities; 1999:705–716.
36. Pinto JT, Suffoletto BP, Berzin TM, et al. Prostate-specific membrane antigen: a novel folate hydrolase in human prostatic carcinoma cells. *Clin Cancer Res*. 1996;2:1445–1451.
37. Perner S, Hofer MD, Kim R, et al. Prostate-specific membrane antigen expression as a predictor of prostate cancer progression. *Hum Pathol*. 2007;38:696–701.